HHS Public Access

Author manuscript

J Mech Behav Biomed Mater. Author manuscript; available in PMC 2016 July 01.

Published in final edited form as:

J Mech Behav Biomed Mater. 2015 July ; 47: 12–20. doi:10.1016/j.jmbbm.2015.03.004.

Correlations between Transmural Mechanical and Morphological Properties in Porcine Thoracic Descending Aorta

Ali Hemmasizadeh[1], **Alkiviadis Tsamis**[4], **Rabee Cheheltani**[1], **Soroush Assari**[1], **Antonio D'Amore**[6], **Michael Autieri**[3], **Mohammad F. Kiani**[1,2], **Nancy Pleshko**[2], **William R. Wagner**[4,6], **Simon C. Watkins**[5], **David Vorp**[4,6], and **Kurosh Darvish**[1,2]

[1]Department of Mechanical Engineering, Temple University, Philadelphia, USA

[2]Department of Bioengineering, Temple University, Philadelphia, USA

[3]Department of Physiology, Temple University, Philadelphia, USA

[4]Department of Bioengineering, University of Pittsburgh, Pittsburgh, PA, USA

[5]Center for Biologic Imaging, University of Pittsburgh, Pittsburgh, PA, USA

[6]McGowan Institute for Regenerative Medicine, University of Pittsburgh, Pittsburgh, PA, USA

Abstract

Determination of correlations between transmural mechanical and morphological properties of aorta would provide a quantitative baseline for assessment of preventive and therapeutic strategies for aortic injuries and diseases. A multimodal and multidisciplinary approach was adopted to characterize the transmural morphological properties of descending porcine aorta. Histology and multi-photon microscopy were used for describing the media layer microarchitecture in the circumferential-radial plane, and Fourier Transform infrared imaging spectroscopy was utilized for determining structural protein, and total protein content. The distributions of these quantified properties across the media thickness were characterized and their relationship with the mechanical properties from a previous study was determined. Our findings indicate that there is an increasing trend in the instantaneous Young's modulus (E), elastic lamella density (ELD), structural protein (SPR), total protein (TPR), and elastin and collagen circumferential Percentage (ECP and CCP) from the inner towards the outer layers. Two regions with equal thickness (inner and outer halves) were determined with significantly different morphological and material properties. The results of this study represent a substantial step toward anatomical characterization of the aortic wall building blocks and establishment of a foundation for quantifying the role of microstructural components on the functionality of aorta.

Corresponding Author: Kurosh Darvish, PhD, Department of Mechanical Engineering, Temple University, 1947 N. 12th Street, Philadelphia, PA 19122, Tel: 215-204-4307 Fax: 215-204-4956 kdarvish@temple.edu.

Conflict of interest

None.

Keywords

Aorta; Nanoindentation; Mechanical Properties; Morphology; Fourier Transform Infrared Imaging Spectroscopy; Multi-Photon Microscopy; Collagen; Elastin; Fiber Orientation

Introduction

Determination of correlations between mechanical and morphological properties of aorta will provide scientists and clinicians with a quantitative baseline for assessment of preventive and therapeutic strategies for traumatic aortic injuries and diseases. Mechanical properties of arteries dictate the normal shape and elasticity of the tissue and changes in these properties are generally associated with important cardiovascular diseases, e.g., transmural delamination and aneurysms (O'Rourke, 1995; Chau and Elefteriades, 2013). Measurement of mechanical properties, however, requires mechanical tests on excised tissues that are not feasible to perform during surgery. Since changes in vascular morphological properties can be determined from various medical imaging techniques *in vivo* (e.g., intravascular ultrasound and intravascular spectroscopy), it is desirable to be able to evaluate the wall mechanical properties from quantified morphological properties. The goal of this study was to determine such correlations in healthy aortic tissue as a first step.

At the microstructural level, the heterogeneous nature of aortic extracellular matrix (ECM) components results in unique characteristics that enable the aorta to maintain its physiological functions (Zou and Zhang 2009). Concentric elastic lamellae are connected by an intricate network of elastin fibrils that form a cage-like structure that surround smooth muscle cells (O'Connell *et al.*, 2008). The lamellae provide the resilience that a large artery needs to absorb the hemodynamic stress of the cardiac systole, and to release this energy in the form of sustained blood pressure during diastole. Collagen fibrils are interspersed in this structure in the form of helically oriented fibers (Holzapfel *et al.*, 2002), which with their high tensile strength, maintain the structural integrity of the vessel and prevent it from excessive deformation. Such interconnections between the ECM components are observed not only in humans but also in other animals; therefore, the aortic microstructure seems to be a universal mechanism that is necessary to maintain the vessel integrity against physiological forces. (Clark and Glagov, 1985; Nakashima and Dis, 2010)

Several studies have shown that the heterogeneity in aortic ECM architecture and components results in significant heterogeneity in the aortic wall mechanical properties (Holzapfel *et al.*, 2005; Matsumoto *et al.*, 2004; Hemmasizadeh *et al.*, 2012). Holzapfel *et al.* (2005) investigated three layers of human coronary arteries with nonatherosclerotic intimal thickening using cyclic quasi-static uniaxial tension tests superimposed on 5% prestretch and found significantly different anisotropic mechanical properties for these layers. Matsumoto *et al.* (2004) developed a scanning micro indentation setup, a scaled-up version of the atomic force microscope (AFM), and determined Young's modulus distribution of the lamellar unit (separated media) of porcine aorta in the longitudinal (LONG) and circumferential (CIRC) directions in the range of 50–180 kPa where the lower and higher values corresponded to the smooth muscle-rich layer and elastic lamina

respectively. Hemmasizadeh *et al.* (2012) used a custom-made nanoindentation technique to characterize changes in the mechanical properties of porcine thoracic aorta wall in the radial (RAD) direction. They distinguished two layers of equal thickness in descending aorta with the outer layer being about 15% stiffer than the inner half.

Changes in the ECM microstructure and components in aorta that occur with cardiovascular diseases such as arteriosclerosis, atherosclerosis, restenosis, hypertension and aortic aneurysms, are generally accompanied with changes in the aorta wall mechanical properties. Studies on pathological effects (Sokolis *et al.* 2002), genetic defects (Brooks *et al.* 2003), phenotypes (Wagenseil *et al.* 2007), and knockout models (Brooks *et al.* 2003) indicated that changes in the ECM components, which in turn represented an early risk factor for cardiovascular disease, were associated with altered mechanical properties. Changes to the ECM components and architecture can also be a result of mechanical loading beyond physiological levels as in hypertension (Lehmann *et al.* 1992) and partial traumatic aortic rupture (Kalita and Schaefer 2007). Therefore, determining the heterogeneity of aortic wall building blocks and characterizing their relationship with the mechanical behavior and properties is particularly important in understanding physiological and pathological conditions in native blood vessels (Guo and Kassab, 2003).

In this study we tested the hypothesis that the heterogeneous mechanical properties of porcine descending thoracic aorta (DTA) wall are correlated with the quantified measures of ECM micro-architecture and protein content across the wall thickness. A multimodal and multidisciplinary approach was adopted to verify this hypothesis. The utilized methods included nanoindentation for measuring local material properties, histology and multi-photon fluorescence microscopy (MFM) for describing the ECM micro-architecture in the CIRC-RAD plane, and Fourier Transform infrared imaging spectroscopy (FT-IRIS) for determining collagen and elastin content, and total protein content.

Materials and Methods

Porcine aorta specimens were used which were excised from sacrificed pigs at a local slaughterhouse immediately post-mortem and submerged in phosphate buffered solution (PBS) and stored in an ice-filled cooler (4°C) while transported to the laboratory. Porcine aorta dimensions, material properties and architecture are similar to human (Wolinsky and Glagov 1967; Garcia *et al.* 2011). Fat and excessive tissues were removed mechanically from the specimens with the careful use of forceps and scalpel. Fifteen 8–10 mm-long cylindrical samples were excised from the descending thoracic aorta of five aortas (3 sections × 5 aorta as shown in Figure 1-a). The LONG locations of the samples were similar to Hemmasizadeh *et al.* (2012) and were above the 1st intercostal artery, between the 1st and 2nd intercostal arteries, and between the 3rd and 4th intercostal arteries respectively. Each sample was fast frozen in an embedding medium (Tissue-Tek O.C.T Compund, Sakura Finetek, Torrance, CA) using liquid nitrogen and were sectioned using a microtome (Leica CM3050S, Norcross, GA). From each sample, slices with three different thicknesses were cut for different types of experiments. 6 μm thickness slices were cut for the histology study, 8 μm thickness for FT-IRIS and 60 μm thickness slices for MFM. The sections were fixed in

formalin after cutting. The total duration of sample preparation, before fixation, was less than 8 hours.

In order to minimize the variability due to CIRC location, all experiments were performed in the medial side of the aorta which is at 90° counter-clockwise with respect to intercostal arteries toward the heart (Figure 1-b). The anatomical location of the tissue across the wall thickness was divided into 10 equal regions and were expressed in terms of a normalized wall thickness r (where $r = 0$ represented the innermost layer and $r = 1$ the outermost layer). About 50 μm from either end of the wall thickness was excluded from further analyses to eliminate any edge effects.

It was shown previously in Hemmasizadeh *et al.* (2012) that the distributions of mechanical properties in the three anatomical locations in the LONG direction (Figure 1-a) were similar. Since the focus of this study was on changes of properties across the aortic wall, and in order to have a larger sample size, the results of these three anatomical locations were combined in the statistical analysis. The experiments were designed such that paired *t*-test was used to compare the quantified properties in the inner and outer halves of the samples. In this manner, variability due to LONG location and inter-specimen variability did not obscure the difference between the two halves. The statistical analyses were conducted in JMP SAS (Version 8, Cary, NC).

Mechanical Properties

The values of transmural instantaneous Young's modulus (E) for porcine DTA were taken from Hemmasizadeh *et al.* (2012). These results were obtained using a nanoindentation technique with a conical indenter at about 50 μm spatial resolution. While the material behavior of aorta is anisotropic and nonlinear for large strains, the value of E represents an effective modulus of the moduli in different directions in the initial linear (toe) region.

Histology

Histological staining was performed to study the transmural changes in the elastic lamellae density (ELD). The Weigert's Resorcin Fuchsin staining was used as it shows the elastic lamellae as dark blue and provides a good contrast between the layers and the surrounding material under light microscope. The images were captured using a Nikon TE200 bright light microscope (Figure 2). The images showed that in the young porcine specimens used in this study, most of the wall thickness consisted of elastic lamellae and therefore can be considered as media. The small intima and adventitia layers were not included in the analyses presented in this paper. The number of elastic lamellae of the aortic media was enumerated for each specimen on microscopic sections under 100× magnification. The ELD (mm^{-1}) in each region was determined by dividing the number of its elastic lamellae by the region's thickness.

Fourier Transform Infrared Imaging Spectroscopy (FT-IRIS)

Aorta cross sections were mounted on MirrIR low-e microscope slides (Kevley Technologies, Chesterland, OH) according to a previously published protocol (Cheheltani *et al.*, 2012). FT-IRIS images were acquired at 25μm pixel resolution and 8 cm^{-1} spectral

resolution with 2 co-added scans using a Perkin Elmer Spotlight 400 spectrometer. Data were analyzed in Isys 5.0 software (Spectral Dimensions Inc, Onley, MD). The integrated area of the Amide I band at ~1640 cm^{-1}, arising primarily from C=O stretching of amide bonds in proteins, was mapped across the tissue sections, creating an intensity image of total protein (Figure 3). This intensity image was imported in Image J (NIH) for further processing. For each sample, a rectangular area of interest from the medial region of the aortic cross section was selected in such a way that included the whole thickness of the aortic wall in width and at least 250 μm in height. Care was taken not to include areas of folding or other histological artifacts. This area of interest was divided into 10 equally spaced smaller sub-regions along the wall thickness, as explained in the previous section, and the mean grey value for each sub-region was measured and reported as TPR (total proteins). This provided 10 relative sequential values of total protein content along aortic wall thickness. The same procedure was repeated for a spectroscopic band centered at 1338 cm^{-1} to map structural proteins, i.e, collagen and elastin and reported as SPR (structural proteins). This band has been observed in the spectra of both collagen and elastin and confirmed with published spectra for these molecules (Cheheltani *et al.*, 2014; Wetzel *et al.*, 2005).

Multi-photon Microscopy

The technique described in Tsamis *et al.* (2013) was implemented to describe the direction of elastin and collagen fibers in the CIRC-RAD plane (Figures 4, 5) of the porcine DTA wall in 10 equally-spaced regions across the thickness. The slices were imaged with the CIRC-RAD plane facing up. Images of collagen and elastin fibers ($0.5\times0.5mm^2$) were processed and fiber directions were assessed with 90° denoting CIRC-orientation and 0° or 180° denoting RAD-orientation (Figure 5). Employing an intensity-based edge detection method (Koch *et al.*, 2014) on images obtained for elastin and collagen fibers of each section, the percentage of CIRC-oriented fiber segments (90°±2.5°) were used to calculate the elastin circumferential percentage (ECP) and the collagen circumferential percentage (CCP) respectively.

Results

The quantified measured parameters including *E*, ELD, SPR, TPR, ECP, and CCP in 10 equally spaced regions across the aorta wall are reported in Table 1. In order to provide a clear picture of the transmural trends of the above parameters, the average values of the quantified parameters were normalized based on their maximum values and plotted in Figure 6. This figure shows that the parameters are generally following the same trend and that they are greater in the outer half of the vessel wall. These observations were further analyzed using linear regression analysis and cluster analysis.

The quantified morphological measurements that were obtained with the same technique were compared and showed a statistically significant and strong correlation between SPR and TPR ($p < 0.0001$, $R^2 = 0.86$) and a significant but relatively weaker correlation between ECP and CCP ($p = 0.0069$, $R^2 = 0.62$).

A cross-correlation validation was conducted for ELD and TPR measures. Based on the aortic wall anatomy, it was expected that the density of elastic lamellae and total protein content would be correlated, i.e., denser regions have more proteins. This correlation was indeed significant ($p = 0.0005$, $R^2 = 0.80$).

A cluster analysis similar to what is described in Hemmasizadeh *et al*. (2012) for E was applied to the other quantified measures and it was concluded that only for ELD a clear cut-off existed between the inner half and the outer half (Figure 7). For the other parameters, the final two clusters did not result in continuous domains in the radial direction.

Based on the cluster analysis results for E and ELD, the hypothesis that $r = 0.5$ acts as a cut-off for the heterogeneity of all quantified parameters was verified using paired t-test. The results are summarized in Table 2, which shows a significant difference between the two halves for all parameters ($p < 0.015$). These results indicate that compared to the inner half, the outer half is mechanically stiffer, the elastic lamellae are denser, total protein and collagen/elastin components are higher, and elastic lamellae and collagen fibers are straighter. For better visualization, the averages of the normalized values for the inner and outer half are shown in Figure 8.

Based on the trends observed in Figure 6, it was hypothesized that a correlation exists between the material properties parameter E, and the rest of the quantified parameters in the form of a multiple regression model. Obtaining such correlation would be significant since it could be used to predict the mechanical properties of aorta based on the microarchitectural geometry and constituent materials. When all five parameters (ELD, SPR, TPR, ECP, and CCP) were included as independent variables, the resulting multiple regression model was not significant. However, since all these parameters are not independent of each other, a principal component analysis (PCA) was performed. To this end, first, linear regression analyses were performed between E and each of the five parameters. It was determined, based on $R^2 > 0.50$, that the strongest correlations were with ELD ($p = 0.0025$, $R^2 = 0.70$), TPR ($p = 0.0133$, $R^2 = 0.58$), and ECP ($p = 0.0066$, $R^2 = 0.62$). In the next step, the principal components were calculated. The normalized data (indicated by subscript N) were used for PCA in order to have the same weight for the three parameters, regardless of their numerical values. The first principal component (eigenvector) was (0.76, 0.49, 0.42), which described 92.4% of the variance of the three parameters. Therefore, a new variable (PC_1) was defined as:

$$PC_1 = 0.76\,\mathrm{ELD}_N + 0.49\mathrm{TPR}_N + 0.42\mathrm{ECP}_N \quad (1)$$

which was used as an independent variable in a linear regression analysis with the normalized Young's modulus (E_N) as the dependent variable. The other principal components that each described less than 5% of the variance were ignored. The linear regression analysis resulted in a significant correlation, $E_N = (0.59 \pm 0.01)PC_1$ ($p < 0.0001$, $R^2 = 0.61$) with the range giving the 95% confidence interval of the coefficient. The normalized relationship between E_N and the normalized three parameters can therefore be written as:

$$E_N = (0.45 \pm 0.01)\,\mathrm{ELD}_N + (0.29 \pm 0.00)\,\mathrm{TPR}_N + (0.25 \pm 0.00)\,\mathrm{ECP}_N \quad (2)$$

This relationship shows that the Young's modulus is more strongly related to the elastic lamellae density and to a lesser extent to the measures of total protein content and horizontal fiber direction of elastin.

Discussion

Characterization of the heterogeneous nature of descending thoracic aortic (DTA) media in the radial direction that was previously addressed with respect to the mechanical properties (Hemmasizadeh *et al.*, 2012) was extended, in this study, to aorta morphology. It was demonstrated that the trends that were observed in the mechanical properties correlated well with quantified morphological parameters. Particularly, the inner and outer halves of DTA media showed distinct morphological properties similar to what was observed for the mechanical properties.

Previous studies on the histology of aortic elastic lamellae have been primarily focused on the organization of the lamellar unit (e.g., Clark and Glagov, 1985) and variation of the average morphology in the LONG direction (e.g., Sokolis *et al.*, 2002). This study showed that the heterogeneity of the lamellar units was also significant in the radial direction and there were more packed and straighter lamellar units in the outer half of the media compared to the inner half. These findings are consistent with the transmural CIRC residual stress. The pioneering work of Chuong and Fung (1986), which has been confirmed by several recent studies (Rachev and Greenwald, 2003; Cardmone et al., 2009), calculated overall compressive residual stresses in the inner wall and tensile residual stresses in the outer wall with the transition happening almost in the middle of the vessel wall. Recent results by Matsumoto *et al.* (2014) also showed that residual stress is inversely related to the waviness of the elastic lamina. Several advantages have been named for the existence of residual stress in arteries including homogenizing the CIRC stress field in the arterial wall, making arteries more compliant, and improving the control of the arterial lumen size by smooth muscle cells (Rachev and Greenwald, 2003).

FT-IRIS has been increasingly used in the past decade for vascular tissue and has emerged as a potential method to determine the biomechanical characteristics of vessel wall and plaques *in vivo*. These include monitoring arterial remodeling after injury (Herman *et al.*, 2009), identification and characterization of vulnerable plaques using characteristic absorption bands of lipids and total protein (Colley *et al.*, 2004; Kazarian and Chan, 2006; Palombo *et al.* 2009), differentiation of normal and aneurysmal human aortas on biopsies of human ascending aortas (Bonnier *et al.*, 2006 and 2008; Rubin *et al.*, 2008), and quantification of collagen and elastin in aortic degradation (Cheheltani *et al.*, 2014). The results of this study showed that the transmural variations of structural proteins and total protein, as measured by FT-IRIS, are consistent with microstructural parameters, and two distinct regions of inner half and outer half could be identified. The region with higher concentration of elastin, collagen, and smooth muscle cells, which are load bearing primarily in tension, coincides approximately with the region with tensile CIRC residual stress.

Therefore, the outer half of aorta media is always in tension, which can partly explain why more load bearing elements are needed in this region.

Tsamis *et al.* (2013) recently used MFM to characterize the elastin and collagen fiber arrangements in the LONG-RAD and CIRC-RAD planes of human non-aneurysmal and aneurysmal ascending thoracic aorta (ATA) tissue specimens. Their samples were artificially dissected in middle of the media. Their analysis of the images provided quantitative fiber microarchitectural characteristics of the media inner and outer halves. While a direct comparison between our study and Tsamis *et al.* (2013) is difficult due to differences in boundary conditions (dissection in mid-media vs. intact media), aorta regions (ATA vs. DTA), and species and age (adult humans vs. young pigs), the values of ECP for the outer half in Tsamis *et al.* (~23%) is about four times as what was found in this study (6.2%). Fung and Liu (1989) showed that, in normal rat aorta, the CIRC residual stress is generally higher in ATA compared to DTA. Based on what was discussed above about the inverse relation of elastic lamellae undulation and residual stress, it can be argued that in ATA, due to the higher level of residual stress, the elastic lamellae would be straighter.

The findings of this study have clinical significance. Understanding how the morphology of aorta affects it mechanical properties and vice versa in intact tissue improves our ability to detect abnormalities in mechanical properties based on changes in morphology. For example, when due to disease (e.g. aneurysm or dissection), the vessel wall morphology is altered, this change can be potentially mapped into changes in mechanical properties. Clearly more experimental data with diseased tissue is needed for such extrapolation. Changes in the mechanical properties can, in turn, be used to predict the progression of these diseases based on biomechanical and remodeling simulations of the vessel wall. A limitation of this study is that the results were obtained for the unloaded state and with only circumferential residual stress. At physiological loaded states with larger strain, the material nonlinearity may become significant. However, it is expected that a similar relationship as Equation (2) but with different coefficients would exist between the local tangent modulus and the morphological parameters.

While the importance of elastin and collagen in the proper function of aorta media is clear (e.g., Nakashima and Dis, 2010; Wagenseil *et al.*, 2009), the results of this study yield quantitative measures and correlations that are essential for modeling applications. With advancement in vascular imaging techniques, e.g., intra-vascular ultrasound (IVUS) or intra-vascular spectroscopy, it will become possible to determine one or more of the quantified measures used in this study for a patient. Using the type of correlations that were derived in this study for human tissue, then the other parameters can be calculated. Due to similarity of porcine and human aorta in morphology and mechanical properties, it is expected that the correlations for human aorta would be similar. A major issue that should be addressed in human aorta is the effect of atherosclerosis and arteriosclerosis. The specimens used in this study represent young and healthy tissues.

In addition to the limitation with respect to the species used and the unloaded state, the presented results are for a specific CIRC location (medial side). It is expected that similar trends exist in other CIRC locations while, due to variations in aorta thickness in the CIRC

direction, the total number of elastic lamellae may be different (Sokolis *et al.*, 2002). Also, the results at three different LONG locations were combined to increase the number of samples. It is expected that the trends of the parameters are similar in DTA regions that are away from branches while the numerical values found for the correlation coefficients (Equation 2) could be different. More data is needed to determine the dependence of the correlation coefficients on the anatomical location.

Conclusions

Three independent methods (Histology, Fourier Transform Infrared Spectroscopy and Multi-photon Microscopy) were utilized to obtain quantified parameters to describe the morphology of porcine DTA across the media layer. These parameters were compared with the heterogeneous material properties. It was demonstrated that the trends that were observed in the mechanical properties also exist in the morphological parameters. Particularly, the inner and outer halves of aorta media showed distinct morphological properties similar to what was observed in the mechanical properties. In general, comparing with the inner half, the outer half was mechanically stiffer, the elastic lamellae were denser, total and structural protein components were higher, and elastic lamellae and collagen fibers were straighter. It was also shown that a statistically significant correlation exists between the instantaneous Young's modulus, and three of the quantified parameters. Young's modulus was more strongly related to the elastic lamellae density and to a lesser extent to the measures of total protein content and horizontal fiber directions of elastin.

Acknowledgments

The guidance of Dr. Farrokh Darvish related to the cluster analysis and PCA used in the study is greatly appreciated. The authors would like to acknowledge funding support of this work by NHLBI under Grant Number K25 HL086512-05 and Grant Number R21 HL088159-02 (KD), and by the Swiss National Science Foundation Fellowships for Advanced Researcher #'s PA00P2_139684 and PA00P2_145399 (AT).

Nomenclature

r	Normalized radial distance
ATA	Ascending thoracic aorta
CCP	Collagen circumferential percentage
CIRC	Circumferential direction
DTA	Descending thoracic aorta
E	Instantaneous Young's modulus
ECM	Extra cellular matrix
ECP	Elastin circumferential percentage
ELD	Elastic lamellae density
LONG	Longitudinal direction
MFM	Multi-photon fluorescence microscopy

PC	Principal component
PCA	Principal component analysis
RAD	Radial direction
SPR	Structural protein content
TPR	Total protein content
subscript *N*	Normalized quantity (divided by the maximum value)

References

Bonnier F, Bertrand D, Rubin S, Venteo L, Pluot M, Baehrel B, Manfait M, Sockalingum GD. Detection of pathological aortic tissues by infrared multispectral imaging and chemometrics. The Analyst. 2008; 133:784–790. [PubMed: 18493680]

Bonnier F, Rubin S, Venteo L, Krishna CM, Pluot M, Baehrel B, Manfait M, Sockalingum GD. In-vitro analysis of normal and aneurismal human ascending aortic tissues using FT-IR microspectroscopy. Biochimica et Biophysica. 2006; 1758:968–973.

Cardamone L, Valentín A, Eberth JF, Humphrey JD. Origin of axial prestretch and residual stress in arteries. Biomech Model Mechanobiol. 2009; 8:431–446. [PubMed: 19123012]

Chau KH, Elefteriades JA. Natural History of Thoracic Aortic Aneurysms: Size Matters, Plus Moving Beyond Size. Progress in Cardiovascular Diseases. 2013; 56(1):74–80.10.1016/j.pcad.2013.05.007 [PubMed: 23993240]

Cheheltani R, McGovern CM, Rao J, Vorp D, Kiani MF, Pleshko N. Fourier transform infrared spectroscopy to quantify collagen and elastin in an in vitro model of extracellular matrix degradation in aorta. Analyst 2014. 2012; 139:3039–3047.

Chuong CJ, Fung YC. On residual stress in artery. J BiomechEng. 1986; 108:189–192.

Clark JM, Glagov S. Transmural organization of the arterial media. The lamellar unit revisited. Arterio- sclerosis. 1985; 5:19–34.

Colley CS, Kazarian SG, Weinberg PD, Lever MJ. Spectroscopic Imaging of Arteries and Atherosclerotic Plaques. Biopolymers. 2004; 74:328–335. [PubMed: 15211501]

Fung YC, Liu SQ. Change of residual strains in arteries due to hypertrophy caused by aortic constriction. Circulation Res. 1989; 65:1340–1349. [PubMed: 2805247]

Garcia E, Laborda PA, Lostale F, De Gregorio MA, Doblare M, Martinez MA. Experimental study and constitutive modelling of the passive mechanical properties of the porcine carotid artery and its relation to histological analysis: Implications in animal cardiovascular device trials. Medical Engineering & Physics. 2011; 33:665– 676. [PubMed: 21371929]

Guo X, Kassab GS. Variation of mechanical properties along the length of the aorta in C57bl/6 mice. American journal of physiology Heart and circulatory physiology. 2003; 285:H2614–H2622. [PubMed: 14613915]

Hemmasizadeh A, Autieri M, Darvish K. Multilayer Material Properties of Aorta Determined from Nanoindentation Tests. Journal of Mechanical Behavior of Biomedical Materials. 2012; 15:199–207.

Herman BC, Kundi R, Yamanouchi BC, Craig Kent K, Liu B, Pleshko N. Molecular analysis of arterial remodeling: a novel application of infrared imaging. SPIE. 2009; 7182:H1–H12.

Holzapfel GA, Gasser TC, Stadler M. A structural model for the viscoelastic behavior of arterial walls: continuum formulation and finite element analysis. European Journal of Mechanics A Solids. 2002; 21:441–463.

Holzapfel GA, Sommer G, Gasser CT, Regitnig P. Determination of layer-specific mechanical properties of human coronary arteries with nonatherosclerotic intimal thickening and related constitutive modeling. The American Journal of Physiology: Heart and Circulatory Physiology. 2005; 289:H2048–H2058.

Kalita P, Schaefer R. Mechanical Models of Artery Walls. Archives of Computational Methods in Engineering. 2007; 15:1–36.

Kazarian SG, Chan KLA. Applications of ATR-FTIR spectroscopic imaging to biomedical samples. Biochimica et Biophysica Acta. 2006; 1758(7):858–867. [PubMed: 16566893]

Koch RG, Tsamis A, D'Amore A, Wagner WR, Watkins SC, Gleason TG, Vorp D. A Custom Image-Based Analysis Tool for Quantifying Elastin and Collagen MicroArchitecture in the Wall of the Human Aorta from Multi-Photon Microscopy. Journal of Biomechanics. 2014; 47(5):935–943. [PubMed: 24524988]

Lehmann ED, Watts GF, Gosling RG. Aortic distensibility and hypercholesterolaemia. Lancet. 1992; 340:1171–1172. [PubMed: 1359256]

Matsumoto, T.; Fukunaga, A.; Narita, K.; Uno, Y.; Nagayama, K. Heterogeneity in Microscopic Residual Stress in the Aortic Wall. In: Barthelat, F., et al., editors. Mechanics of Biological Systems and Materials; Proceedings of the 2013 Annual Conference on Experimental and Applied Mechanics; 2014. p. 99-106.

Matsumoto T, Goto T, Furukawa T, Sato M. Residual stress and strain in the lamellar unit of the porcine aorta: Experiment and analysis. Journal of Biomechanics. 2004; 37:807–815. [PubMed: 15111068]

Nakashima Y, Dis AN. Pathogenesis of Aortic Dissection: Elastic Fiber Abnormalities and Aortic Medial Weakness. Annals of Vascular Diseases. 2010; 3(1):28–36. [PubMed: 23555385]

O'Rourke M. Mechanical Principles in Arterial Disease. Hypertension. 1995; 26:2–9.10.1161/01.HYP.26.1.2 [PubMed: 7607724]

O'Connell MK, Murthy S, Phan S, Xu C, Buchanan J, Spilker R, Dalman RL, Zarins CK, Denk W, Taylor CA. The three-dimensional micro and nanostructure of the aortic medial lamellar unit measured using 3D confocal and electron microscopy imaging. Matrix Biology. 2008; 27:171–181. [PubMed: 18248974]

Palombo F, Cremers SG, Kazarian SG, Weinberg PD. Application of Fourier transform infrared spectroscopic imaging to the study of effects of age and dietary L-arginine on aortic lesion composition in cholesterol-fed rabbits. Journal of the Royal Society Interface. 2009; 6:669–680.

Rachev A, Greenwald SE. Residual strains in conduit arteries. Journal of Biomechanics. 2003; 36:661–670. [PubMed: 12694996]

Rubin S, Bonnier F, Sandt C, Venteo L, Pluot M, Baehrel B, Manfait M, Sockalingum GD. Analysis of Structural Changes in Normal and Aneurismal Human Aortic Tissues Using FTIR Microscopy. Biopolymer. 2008; 89:160–169.

Sokolis DP, Boudoulas H, Kavantzas NG, Kostomitsopoulos N, Agapitos EV, Karayannacos PE. A morphometric study of the structural characteristics of the aorta in pigs using an image analysis method. Anatomia Histologia Embryologia Journal of Veterinary Medicine Series C. 2002; 31(1):21–30.

Tsamis A, Phillippi JA, Koch RG, Pasta S, D'Amore A, Watkins SC, Wagner WR, Gleason TG, Vorp DA. Fiber micro-architecture in the longitudinal-radial and circumferential-radial planes of ascending thoracic aortic aneurysm media. Journal of Biomechanics. 2013; 46 (16):2787–2794. [PubMed: 24075403]

Wagenseil JE, Ciliberto CH, Knutsen RH, Levy MA, Kovacs A, Mecham RP. Reduced Vessel Elasticity Alters Cardiovascular Structure and Function in Newborn Mice. Circulation Research. 2009; 104:1217–1224. [PubMed: 19372465]

Wagenseil JE, Knutsen RH, Li D, Mecham RP. Elastin insufficient mice show normal cardiovascular remodeling in 2K1C hypertension, despite higher baseline pressure and unique cardiovascular architecture. American journal of physiology. Heart and circulatory physiology. 2007; 293:H574–H582. [PubMed: 17400710]

Wetzel DL, Wetzel LH, Wetzel MD, Lodder RA. Imminent cardiac risk assessment via optical intravascular biochemical analysis. Analyst. 2009; 134(6):1099–1106. [PubMed: 19475135]

Wolinsky H, Glagov S. A Lamellar Unit of Aortic Medial Structure and Function in Mammals. Circulation Research. 1967; 20:99–111. [PubMed: 4959753]

Zou Y, Zhang Y. An experimental and theoretical study on the anisotropy of elastin network. Annals of Biomedical Engineering. 2009; 37:1572–1583. [PubMed: 19484387]

Author Manuscript

Author Manuscript

Author Manuscript

Highlighted

- Mechanical and morphological properties of porcine aorta wall were characterized.
- Two halves of the media had significantly different properties.
- Material properties were described in terms of morphological properties.

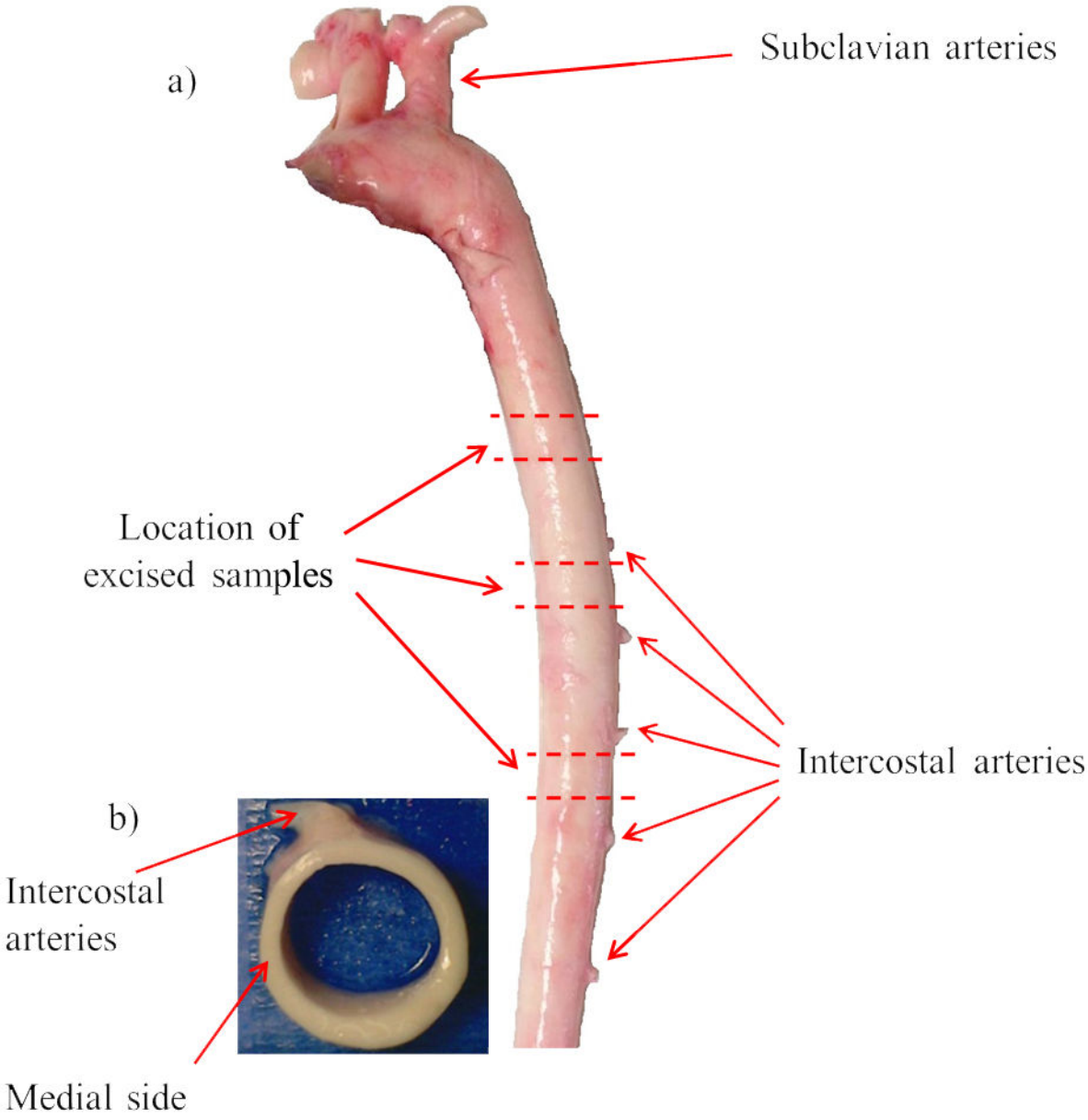

Figure 1.

a) Location of excised samples along the descending thoracic porcine aorta. b) Top view of a cylindrical section. Location of experiments across the wall thickness in the medial side of aorta is shown which is at 90° counter-clockwise with respect to intercostal arteries toward the heart.

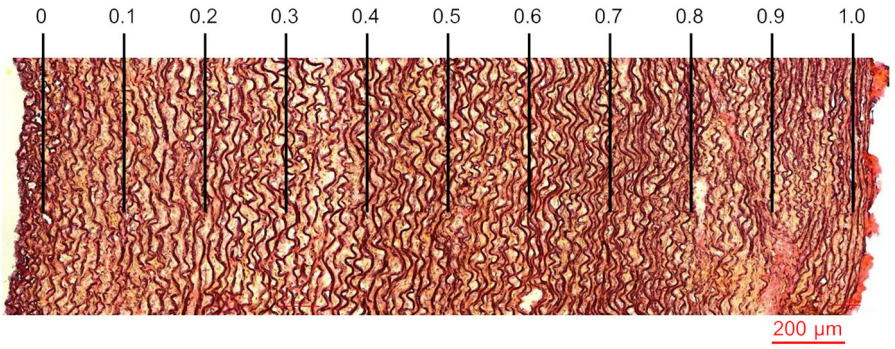

Figure 2.

Weigert's Resorcin Fuchsin staining to study transmural changes of the elastic lamellae density (ELD) in media. Categorization of the region of interest into 10 equal sub-regions based on the normalized wall thickness r is shown. Lumen is at the left side.

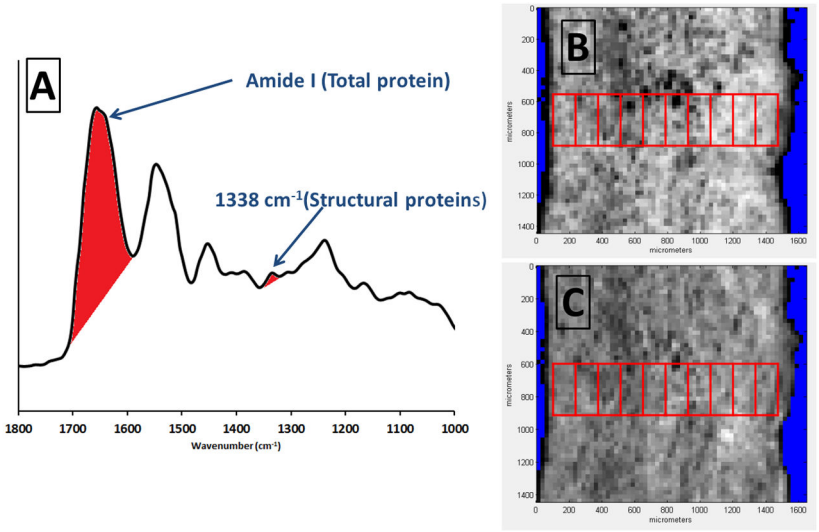

Figure 3.

a) Peak integration of amide I band for mapping total protein content and the band centered at 1338 cm^{-1} for mapping structural proteins (collagen and elastin), b) Intensity image of total protein content from peak integration mapping of amide I band in a typical sample and selection of region of interest and sub-regions. c) Intensity image of structural proteins from peak integration mapping of the 1338 cm^{-1} band in the same sample and selection of region of interest and sub-regions.

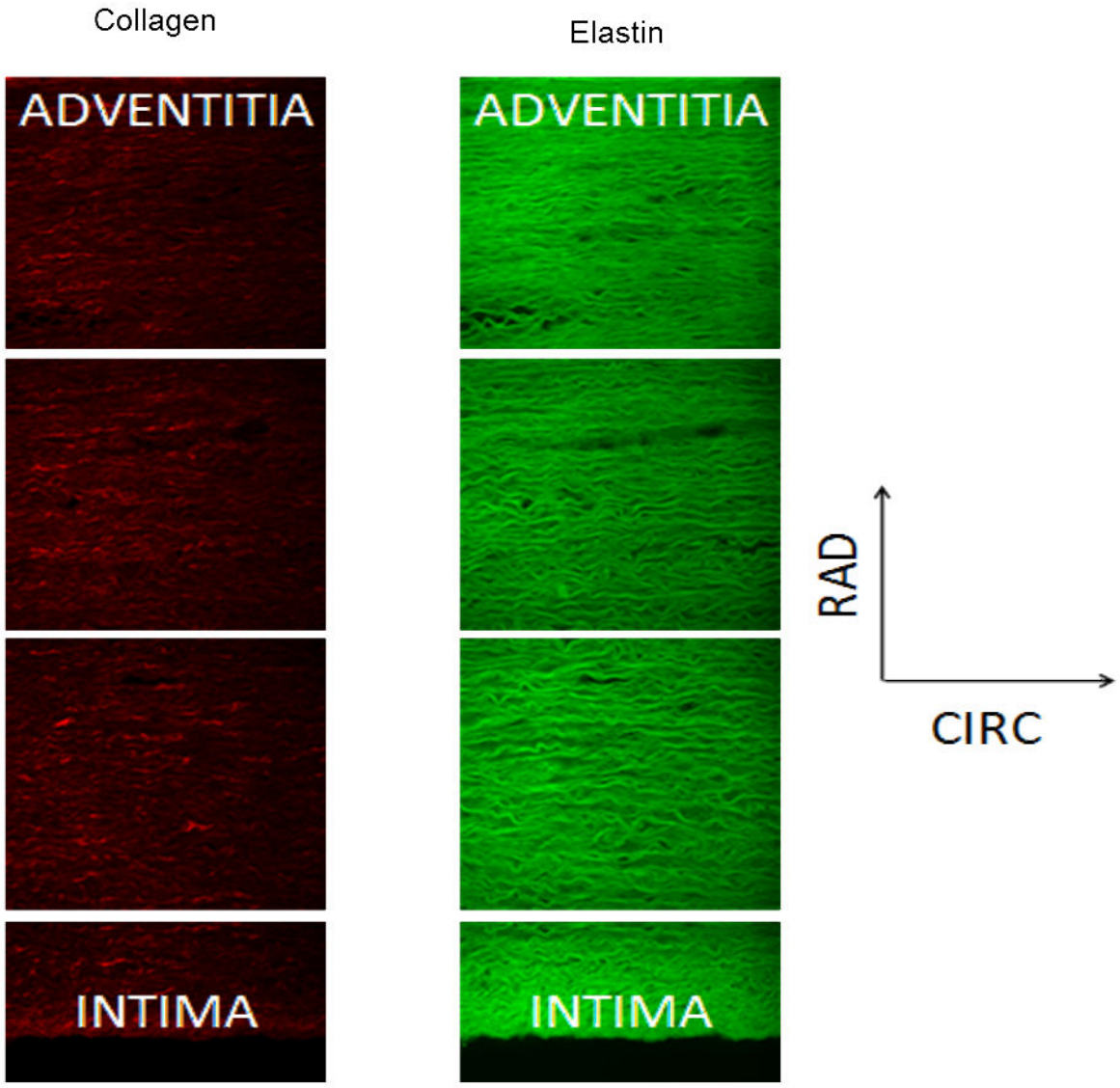

Figure 4.

Representative MFM images across the descending thoracic porcine aorta wall in the CIRC-RAD plane for collagen (left) and elastin (right).

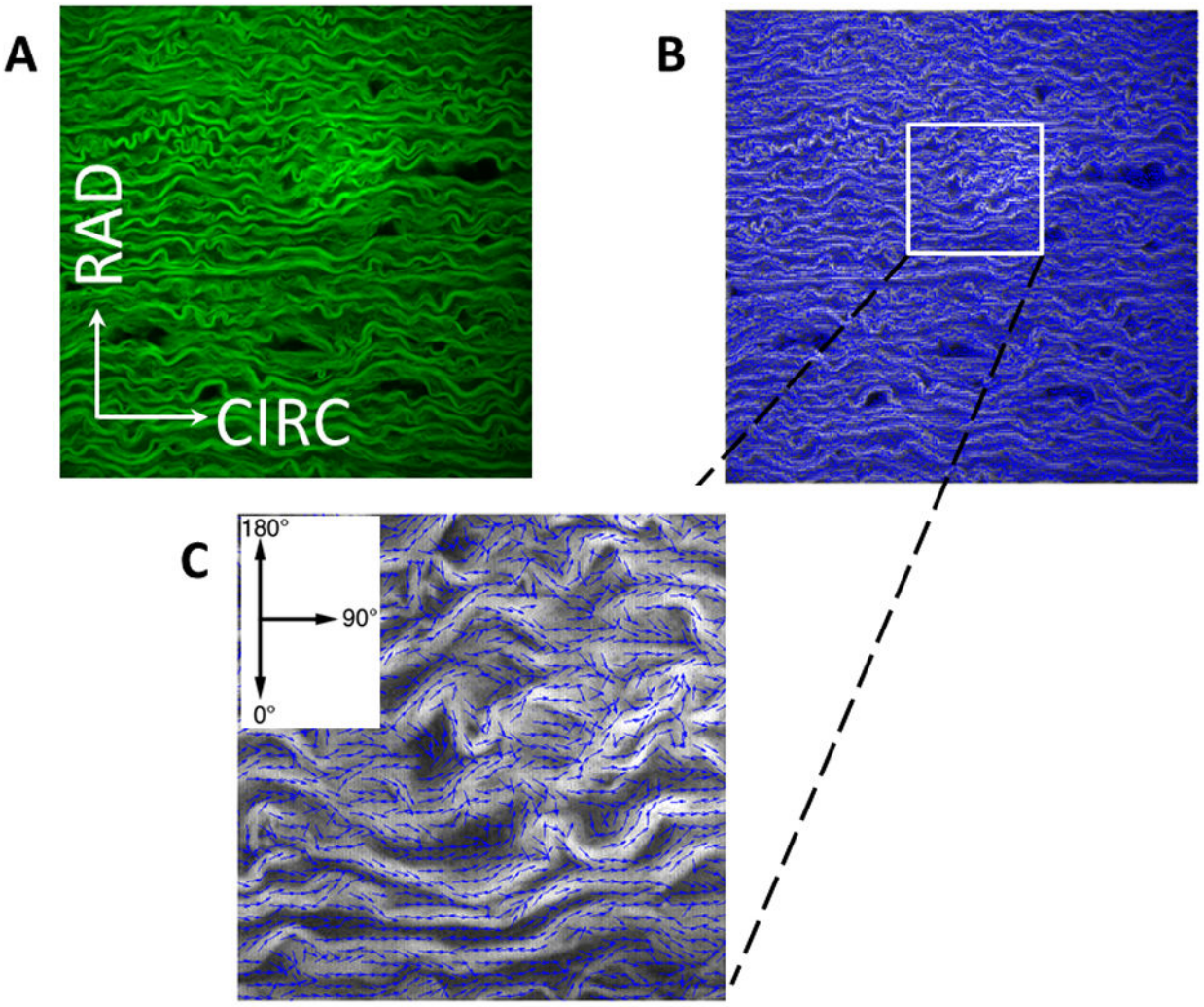

Figure 5.

A) Example of analysis of MFM image ($0.5\times0.5mm^2$) of elastin fibers of porcine DTA media in CIRC-RAD plane. B) Processed image with fiber segments represented by small arrows in blue that follow the direction of the fibers. C) A higher magnification of a small area of (B). The percentage of fiber segments that were in the 90°±2.5° direction were used for ECP and CCP calculations.

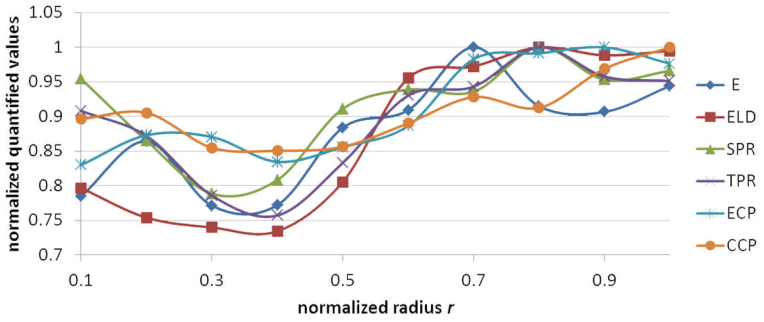

Figure 6.

Trends of normalized aorta quantified parameters across media listed in Table 1 with respect to the normalized radius. The parameters are normalized by dividing to their maximum value.

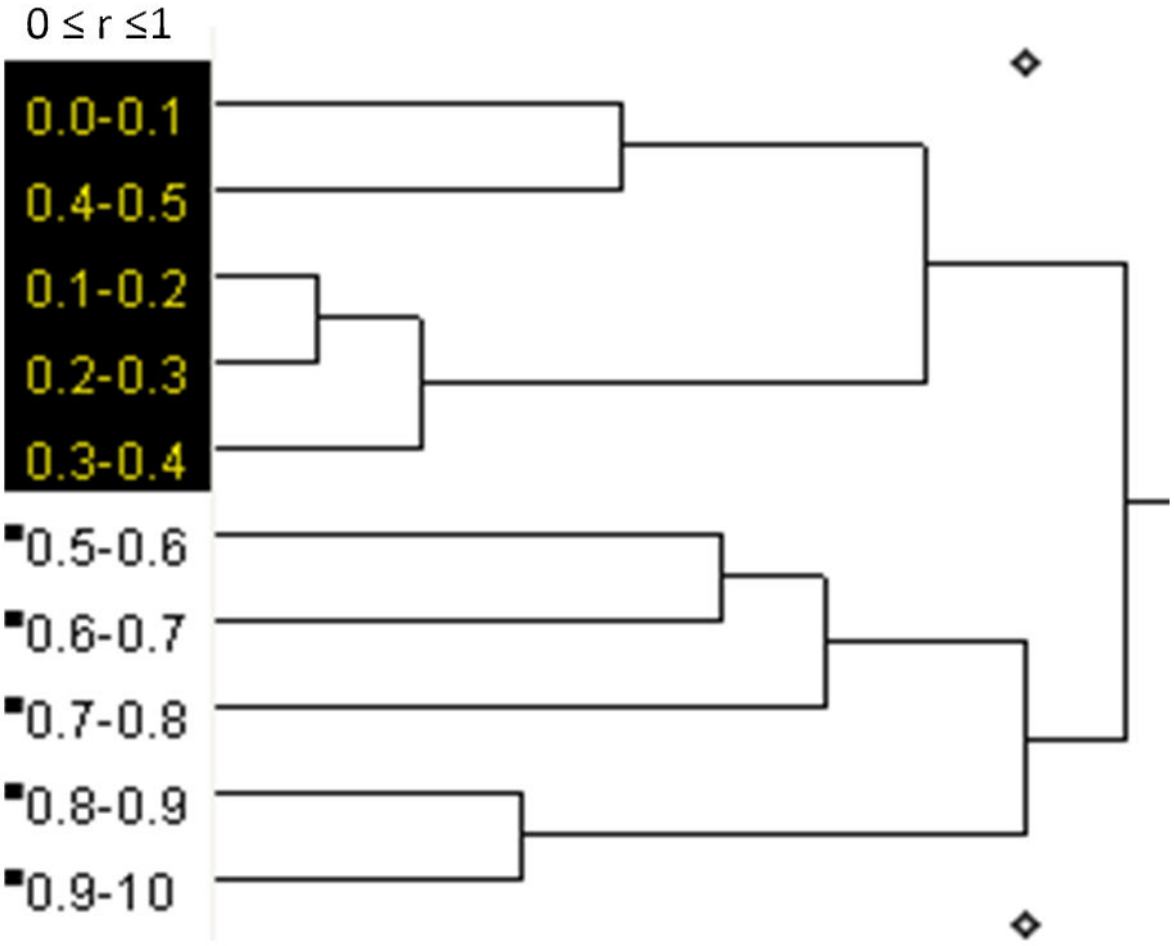

Figure 7.

The dendrogram result of ELD from applying hierarchical cluster analysis. The results show that 10 regions of r used in this study were combined in several steps and at the end, two regions were distinguishable with one containing the inner half of the wall thickness (r = 0.0–0.5) and the other the outer half (r = 0.5–1.0).

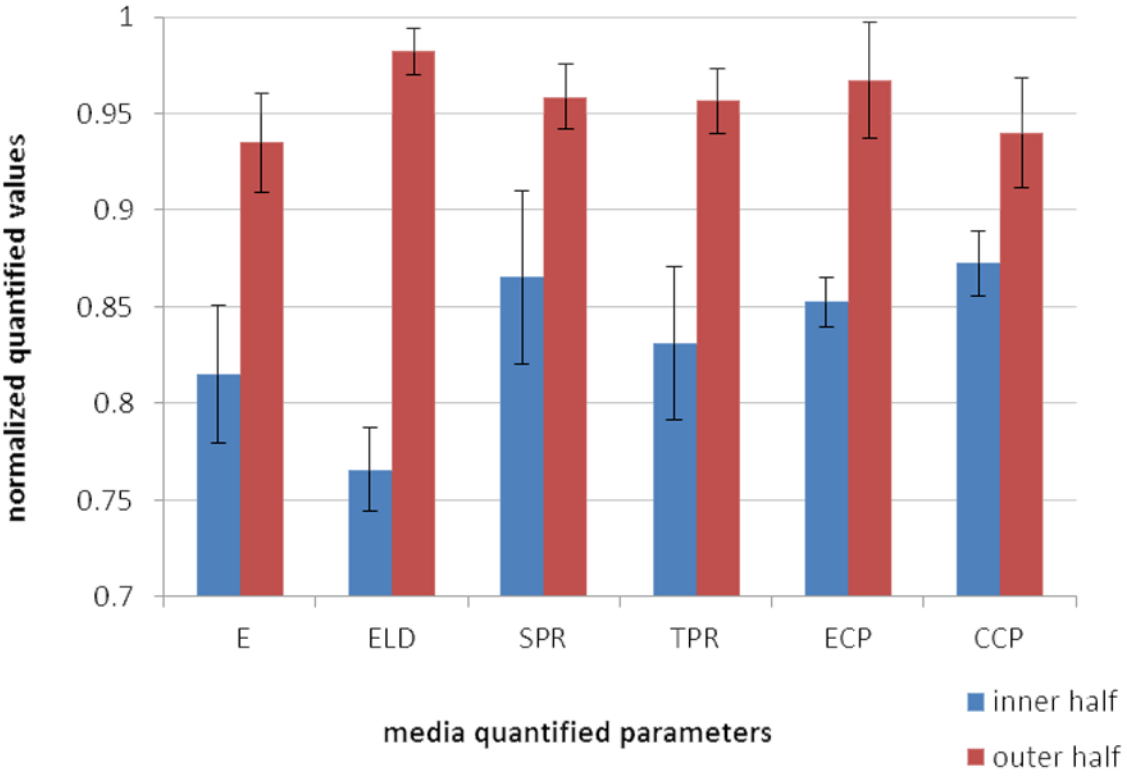

Figure 8.

Average normalized quantified parameters for the inner and outer halves of the media. Error bars show 95% confidence intervals.

Table 1

Media layer quantified transmural parameters given as average (standard deviation) with *n*= 15: E (Young's modulus), ELD (elastic lamellae density), SPR (structural proteins), TPR (total proteins), ECP (elastin CIRC percentage), and CCP (collagen CIRC percentage).

Normalized Distance	E (kPa)	ELD (mm-1)	SPR (arbitrary unit)	TPR (arbitrary unit)	ECP (%)	CCP (%)
0.0–0.1	57.98 (10.14)	53.23 (8.17)	125.14 (32.33)	169.47 (22.15)	5.32 (1.26)	4.67 (0.78)
0.1–0.2	63.82 (14.68)	50.36 (13.01)	113.41 (29.01)	162.73 (18.22)	5.60 (1.31)	4.72 (0.93)
0.2–0.3	56.94 (9.18)	49.41 (10.58)	103.36 (24.03)	146.63 (18.72)	5.58 (0.98)	4.46 (0.63)
0.3–0.4	57.02 (10.26)	49.05 (8.15)	105.96 (20.43)	141.28 (28.62)	5.35 (0.95)	4.43 (0.62)
0.4–0.5	65.29 (18.14)	53.81 (6.53)	119.44 (17.52)	155.46 (19.65)	5.49 (1.13)	4.46 (0.63)
0.5–0.6	67.16 (25.97)	63.84 (12.70)	123.07 (22.14)	173.62 (18.39)	5.68 (1.19)	4.64 (0.69)
0.6–0.7	73.87 (22.09)	64.97 (8.91)	122.70 (31.13)	176.02 (24.00)	6.30 (1.61)	4.84 (0.76)
0.7–0.8	67.57 (19.35)	66.82 (10.90)	131.11 (24.75)	186.63 (12.27)	6.36 (1.75)	4.76 (0.85)
0.8–0.9	66.96 (17.68)	66.04 (8.67)	124.97 (29.35)	178.73 (18.46)	6.41 (1.60)	5.05 (0.69)
0.9–1.0	69.72 (15.01)	66.46 (10.07)	126.64 (27.56)	177.55 (21.33)	6.26 (1.46)	5.21 (0.79)

J Mech Behav Biomed Mater. Author manuscript; available in PMC 2016 July 01.

Table 2

Average values of quantified parameters for inner half and outer half regions of the media with their 95% confidence intervals, percentage of changes from the inner to the outer half, and *p*-values for paired two-tail *t*-tests between the two halves.

	E (kPa)	ELD (mm-1)	SPR (arbitrary unit)	TPR (arbitrary unit)	ECP (%)	CCP (%)
Inner Half	60.21 ± 2.61	51.17 ± 1.43	113.46 ± 5.89	155.11 ± 7.44	5.47 ± 0.08	4.55 ± 0.09
Outer Half	69.06 ± 1.88	65.62 ± 0.79	125.70 ± 2.21	178.51 ± 3.19	6.20 ± 0.19	4.90 ± 0.15
Percentage of change	15	28	11	15	13	8
p-value	0.001	<0.0001	0.015	<0.0001	0.003	0.010